Atmos. Chem. Phys., 14, 159–174, 2014
www.atmos-chem-phys.net/14/159/2014/
doi:10.5194/acp-14-159-2014

Atmospheric Chemistry and Physics Open Access

Mesoscale modeling of smoke transport over the Southeast Asian Maritime Continent: coupling of smoke direct radiative effect below and above the low-level clouds

C. Ge[1,2], **J. Wang**[1], **and J. S. Reid**[3]

[1]Department of Earth and Atmospheric Sciences, University of Nebraska – Lincoln, NE, USA
[2]State Key Laboratory of Atmospheric Boundary Layer Physics and Atmospheric Chemistry, Institute of Atmospheric Physics, Chinese Academy of Sciences, Beijing, China
[3]Naval Research Laboratory, Monterey, CA, USA

Correspondence to: J. Wang (jwang7@unl.edu)

Received: 7 April 2013 – Published in Atmos. Chem. Phys. Discuss.: 11 June 2013
Revised: 4 November 2013 – Accepted: 27 November 2013 – Published: 6 January 2014

Abstract. The online-coupled Weather Research and Forecasting model with Chemistry (WRF-Chem) is used to simulate the direct and semi-direct radiative impacts of smoke particles over the Southeast Asian Maritime Continent (MC, 10° S–10° N, 90–150° E) during October 2006 when a significant El Niño event caused the highest biomass burning activity since 1997. With the use of an OC (organic carbon) / BC (black carbon) ratio of 10 in the smoke emission inventory, the baseline simulation shows that the clouds can reverse the negative smoke forcing in cloud-free conditions to a positive value. The net absorption of the atmosphere is largely enhanced when smoke resides above a cloud. This led to a warming effect at the top of the atmosphere (TOA) with a domain and monthly average forcing value of $\sim 20\,\mathrm{W\,m^{-2}}$ over the islands of Borneo and Sumatra. Smoke-induced monthly average daytime heating (0.3 K) is largely confined above the low-level clouds, and results in a local convergence over the smoke source region. This heating-induced convergence transports more smoke particles above the planetary boundary layer height (PBLH), hence rendering a positive effect. This positive effect contrasts with a decrease in the cloud fraction resulting from the combined effects of smoke heating within the cloud layer and the more stable boundary layer; the latter can be considered as a negative effect in which a decrease of the cloud fraction weakens the heating by smoke particles above the clouds. During the nighttime, the elevated smoke layer lying above the clouds in the daytime is decoupled from the boundary layer, and the enhanced downdraft and shallower boundary layer lead to the accumulation of smoke particles near the surface. Because of monthly smoke radiative extinction, the amount of solar input at the surface is reduced by as much as $60\,\mathrm{W\,m^{-2}}$, which leads to a decrease in sensible heat, latent heat, 2 m air temperature, and PBLH by a maximum of $20\,\mathrm{W\,m^{-2}}$, $20\,\mathrm{W\,m^{-2}}$, 1 K, and 120 m, respectively. During daytime, the cloud changes over continents mostly occur over the islands of Sumatra and Borneo where the low-level cloud fraction decreases more than 10 %. However, the change of local wind, including sea breeze, induced by the smoke direct radiative effect leads to more convergence over the Karimata Strait and the south coastal area of Kalimantan during both daytime and nighttime; consequently, the cloud fraction there is increased up to 20 %. The sensitivities with different OC / BC ratios show the importance of the smoke single-scattering albedo for the smoke semi-direct effects. Lastly, a conceptual model is used to summarize the responses of clouds, smoke, temperature, and water vapor fields to the coupling of smoke direct effect below and above clouds over the Southeast Asian Maritime Continent.

1 Introduction

In September and October of 2006, moderate El Niño conditions resulted in negative precipitation anomalies in the Southeast Asian Maritime Continent (MC, 10° S–10° N, 90–

150° E). Subsequent drought conditions then led to the most significant biomass burning activity since the massive 1997 event that first drew attention to the region (van der Werf et al., 2008; Reid et al., 2012). For the first time, a large El Niño-induced burning season could be observed by NASA's afternoon or A-train satellite constellation and thus be characterized by models with advanced data assimilation. In total, ~ 3.5 Tg smoke particles were emitted according to the Fire Locating and Modeling of Burning Emissions (FLAMBE) estimate (Reid et al., 2009; Wang et al., 2013). Fires in Sumatra and Borneo contributed to a 24 h mean near-surface PM_{10} concentration above 150 mg m^{-3} at multiple locations in Singapore and Malaysia over several days (Hyer and Chew, 2010; Wang et al., 2013).

This study investigates the radiative effect of smoke particles on planetary boundary layer (PBL) properties during October 2006 in the MC when regional smoke concentrations and aerosol optical depths (AODs) had been at a regional maximum for the last decade (Reid et al., 2012; Wang et al., 2013; Xian et al., 2013). Indeed, Moderate Resolution Imaging Spectroradiometer (MODIS) average clear-sky mid-visible AODs were over 0.8 for a large band stretching from Sumatra through Borneo for this period (Xian et al., 2013). A study of this period would provide an upper-end benchmark on aerosol radiation interaction in the region. The significance of the smoke radiative effect over the Asian MC has also been recognized by several past studies, both from satellite data and global chemistry models (e.g., Duncan, 2003; Podgorny et al., 2003; Davison et al., 2004; Parameswaran et al., 2004; Rajeev, 2004; Thampi et al., 2009; Ott et al., 2010). Based on a radiative transfer model, Podgorny et al. (2003) studied aerosol radiative forcing of the 1997 Indonesia forest fire and showed that the low-level clouds embedded in the absorbing aerosols increased aerosol-induced absorption in the troposphere, and decreased the magnitude of aerosol forcing at the top of the atmosphere (TOA) (also see Ramanathan et al., 2001). They concluded that relatively small changes in low-level cloud fractions and single-scattering albedo (SSA) might result in significant changes in the magnitude and even in the sign (positive or negative) of the TOA forcing.

As discussed in Reid et al. (2012, 2013) and Wang et al. (2013), the distribution of smoke particles over the MC is affected by an interplay of several meteorological systems at various temporal and spatial scales, including the El Niño–Southern Oscillation (ENSO), the Intertropical Convergence Zone (ITCZ)/monsoon and trade winds at larger scales, the Madden–Julian oscillation (MJO) and typhoons at mesoscale, and the sea breezes, topography and boundary layer process at local scales. Differing from previous analyses, our focus here is to investigate the impacts of smoke direct radiative effects on meteorology at regional to local scales. This study is the second part of a series of our mesoscale modeling efforts for the 7 Southeast Asian Studies (7SEAS) Project, among many other research goals, to reveal the production, transport and radiative effects of aerosols in MC (Campbell et al., 2013; Feng and Christoipher, 2012; Hyer et al., 2012; Reid et al., 2012, 2013; Salinas et al., 2013; Wang et al., 2013; Xian et al., 2013). Wang et al. (2013) used WRF-Chem in conjunction with satellite data and ground-based $PM_{2.5}$ data to identify the smoke transport pathway under the influence of aforementioned multi-scale meteorological factors. Here, we examine the radiative impacts of smoke particles from the same mesoscale simulations.

It is well known that the direct radiative effect of smoke particles depends highly on the smoke single-scattering albedo, smoke amount or smoke AOD, not only in column layers but also in different vertical layers (Wang and Christopher, 2006, and references therein). Specific to the MC smoke particles, their single-scattering properties have not been well studied (Davison et al., 2004; Reid et al., 2013), although past analyses (such as Tosca et al., 2011; Campbell et al., 2013; Wang et al., 2013, and references therein) have shown that smoke particles are primarily located within or just above the boundary layer (~ 1.5–2 km above the surface). Our current study is designed to conduct a series of numerical experiments with perturbations in particle single-scattering characteristics, and evaluate how smoke's radiative effects can influence boundary layer properties such as air temperature, sensible and latent heat fluxes, boundary layer height and cloud cover in a complex meteorological environment such as in MC. The goal of the paper is to relate possible physical mechanisms at regional-to-local scales, rather than to quantify exactly the impact of the smoke radiative effect; the latter certainly will not be likely until the aerosol optical properties are well characterized in the conclusion of the 7SEAS field campaign.

While the single-scattering albedo of smoke particles is known to be highly dependent on its relative composition of black carbon and organic mass (Reid et al., 2005a), the dearth of in situ measurements for characterizing the smoke properties in MC make it impossible for us to find an optimal OC (organic carbon) / BC (black carbon) ratio to use in the simulation (Reid et al., 2013). Instead, we conducted the WRF-Chem simulation with a set of OC / BC ratios in smoke emissions, and analyzed the sensitivity of smoke direct radiative effect to different OC / BC ratios. We describe the experiment design, including the WRF-Chem model and data used in this study, in Sect. 2, and present the baseline modeled results of the smoke radiative impact on surface energy budget and the associated dynamics processes in Sect. 3. In Sect. 4, we describe the conduction of model sensitivity simulations to ascertain the impact of smoke with different OC / BC ratios. A conceptual model that illustrates the finding of this study is given in Sect. 5, while itemized summaries are provided in Sect. 6.

Table 1. Configuration options employed by WRF-Chem in this study.

Atmospheric Process	Model Option
Longwave radiation	RRTM scheme (Mlawer, 1997)
Shortwave radiation	GSFCSW model
Surface layer	MM5
Land surface	Noah
Boundary layer	YSU (Hong et al., 2006)
Cumulus clouds	G3 (Grell and Devenyi, 2002)
Cloud microphysics	Lin (Lin et al., 1983)
Gas-phase chemistry	RADM2 (Stockwell et al., 1990)
Aerosol chemistry	MADE/SORGAM (Ackermann et al., 1998; Schell et al., 2001).
Optical module	Volume mixing rule ((Bond and Bergstrom, 2006)
Horizontal resolution	81 km for outer domain, 27 km for inner domain (Fig. 1)
Vertical layers	27

2 Model description

2.1 Configuration of WRF-Chem

The WRF-Chem model (Fast et al., 2006; Grell et al., 2005) can be used for weather forecasting and regional climate studies as well as to simulate gas-phase chemistry, aerosol life cycles, and aerosol–cloud–radiation interactions. The model configuration in this study is similar to Wang et al. (2013), and Table 1 lists the model configuration options employed in this study. Wang et al. (2013) showed that, when FLAMBE smoke emissions are injected within 800 m above the surface, a good agreement can be found between the simulation of WRF-Chem and satellite/ground-based observations in terms of surface $PM_{2.5}$ mass, aerosol vertical profile, and smoke transport path. However, while similar model configurations (to those in Wang et al., 2013) will be used for the numerical experiments in this study, this study differs from Wang et al. (2013) in that both the smoke direct-radiative effect and the semi-direct effect are studied, and the impact of uncertainty in smoke single-scattering albedo is investigated. Generally, besides the direct effects of scattering and absorbing incoming solar radiation, aerosols can indirectly influence the climate by acting as cloud condensation nuclei (CCN) and/or ice nuclei (CN) that modify the microphysical, radiative properties and lifetime of clouds. Several studies (e.g. Reid et al., 1998; Koren et al., 2008) imply that indirect effects dominate under clean conditions, while aerosol radiative effects become more important under heavily polluted conditions. During our study period, the concentration of $PM_{2.5}$ was always high over MC (Wang et al., 2013), and although the aerosols' indirect effect is very important, its perturbation at such a high particle-loading condition might not be as sensitive as that of the direct effect, especially over smoke source regions. The indirect effects might become critically prominent over the area further out from the MC, and, therefore, we plan to study them further in the future.

It is worth noting that only smoke particle emissions, portioned as BC and OC, is considered in the current WRF-Chem simulation. As shown in Wang et al. (2013), smoke emission dominates other emissions, e.g., industrial emissions, in September–October 2006, and therefore, to be consistent with our interest in smoke radiative effects and also to avoid large uncertainties in the simulation of secondary organic aerosols, the emission from other sources – including industrial emission, biogenic emission, and wind-blow sea salt – are not implemented in the simulation. Our experiment design follows the strategy used by Wang and Christopher (2006) where they studied the radiative impact of Central American smoke particles by only considering the smoke particle emission. Similar to Wang et al. (2013), the smoke emission inventory from FLAMBE is used to specify the source of BC and OC (with different BC and OC emission ratios as described in the following section) as a function of time (with updates of every 6 h). In the model, the injection height of smoke (OC and BC) emissions is specified as 800 m above the surface, and within this injection height the emissions are uniformly distributed (Wang et al., 2013).

The $1^\circ \times 1^\circ$ National Center for Environmental Prediction (NCEP) Final Analysis (FNL) data at 00:00, 06:00, 12:00 and 18:00 UTC are used for initializing and specifying the temporally evolving lateral boundary conditions. The time-varying sea surface temperature (SST), sea ice, vegetation fraction, and albedo were updated every 6 h from the NCEP reanalysis data during the model simulation. We noticed that the use of 6 h nudged SST may not be ideal for studying the response of SST to the smoke aerosol radiation interaction. However, this non-ideality has to be compromised because of the lack of a fully coupled ocean model within WRF-Chem. Furthermore, as shown in Wang et al. (2013), most smoke particles are over the land and the ocean close to the Southeast Asian Maritime Continent, and so a large-scale change of SST due to smoke radiative effects is unlikely. In addition, the temperature contrast between coastal ocean and land is well demonstrated by the simulated sea and land

breezes (Wang et al., 2013). This also partly supports the use of nudged SST in analyzing smoke radiative effects, which, while not ideal, is reasonable for this study.

According to the database compiled by Barnard et al. (2010), and also as described in Zhao et al. (2010), the shortwave refractive index for BC and OC is not wavelength dependent in this study. The refractive index of BC in this study is assigned the value of $1.95+i0.79$ for both shortwave and longwave. The refractive index of OC (dry) is 1.45 for shortwave, and for longwave it is in the range of 1.22–2.50 (real part) and 0.01–0.5 (imaginary part). The density of BC and OC is assumed to be $1.7\,\mathrm{g\,cm^{-3}}$ and $1\,\mathrm{g\,cm^{-3}}$, respectively. The hygroscopicity (size growth factor) is assumed to be 0.14 for OC and a very small nonzero value (10^{-6}) for BC (Ghan et al., 2001), and hence the wet mode radius for BC can be diagnosed from RH, hygroscopicity and other related parameters. The optical properties are computed with Mie parameterizations that are a function of wet surface mode radius and refractive indices of wet aerosols in each mode (Zhang, 2008). The size distributions of OC and BC emissions are both represented as an accumulation mode with a mean volume diameter of 0.3 µm and a standard deviation of 2.

2.2 Experiment design

The relative mass fraction of BC and OC in smoke particles can vary significantly, depending on the composition of the biomass burned, the fire temperature regulating the phases of flaming and smoldering in the combustion, and the particle age (Andreae and Merlet, 2001; Kleeman et al., 2000; Liousse et al., 1996; Reid et al., 2005b, 2012, 2013). Although BC typically accounts for 4–8 % smoke particle dry mass and approximately 50–65 % of mass is attributable to organic carbon, the review by Reid et al. (2012) showed very large differences in the literature-reported particle properties, in particular with regards to particle carbon budgets. In the study of Akagi et al. (2011), emission factor of BC and OC from tropical forest is 0.52 and $4.71\,\mathrm{g\,kg^{-1}}$, respectively, with a corresponding estimate of the natural variation of 0.28 and 2.73, and emission factors of BC and OC from peatland can be 0.20 and 6.23 with variation of 0.11 and 3.60, respectively. He admitted that large uncertainties still exist for these emission factors because only a limited number of fire types and smoke-processing scenarios have been sampled with currently available instruments. In this study, three ratios of OC / BC as 3.5, 10 and 17 are selected and used in WRF-Chem. In doing so, we can obtain a wider range in model climate response, thus offering a perspective on the radiative impacts of BC aerosols over the Southeast Asian Maritime Continent. Four sets of simulations are performed in this study and the detail can be seen in Table 2. In all simulations, the total amount of emitted particulate organic matter ($1.5 \times$ OC mass) and BC amount are kept at the same 90 % of the total smoke particle mass that is estimated in FLAMBE, and consistent with Herner et al. (2005), Lim and Turpin (2002). The remaining 10 % of the total smoke particle mass is not considered in the simulation since the uncertainty of the optical property of those masses could be quite large. All numerical simulations are initiated at 00:00 UTC on 20 September 2006, and ended at 00:00 UTC on 2 November 2006. However, only data during 1–31 October 2006 are analyzed, during which time the most smoke events occurred (Wang et al., 2013). Except in Fig. 9b, all variables in the analysis are monthly averages of October 2006.

Table 2. Experiments design.

	Baseline	S1	S2	S3
OC / BC	10	3.5	17	10
BC/particle mass	5.6 %	15.6 %	3.3 %	5.6 %
Aerosol radiative effect	yes	yes	yes	no

3 Baseline results (OC / BC = 10)

3.1 Smoke radiative effect at surface and TOA

Monthly averaged aerosol, radiation, and cloud features for October 2006 are presented in Fig. 1. This corresponds to a post-monsoonal shift and regional drying event that leads to the largest El Niño-based fire events in the region (Reid et al., 2012). Discussion of regional meteorology for this specific period can be found in Wang et al. (2013). Two regions with high AOD and high absorption aerosol optical depth (AAOD) values are found in the monthly mean (all-sky condition) of model simulations (Fig. 1a and b); they are respectively located at the Kalimantan and the Sumatra regions with large fire emissions (Wang et al., 2013) and relatively low topography (Fig. 1c). The all-sky AOD average in this study at these locations is 30–50 % lower than that from MODIS AOD retrievals (as showed in Xian et al., 2013). One reason is MODIS AOD is only reliable in clear-sky conditions, but the model simulation is all-sky AOD (Zhang and Reid, 2009). Another reason for smaller simulated AOD is that only smoke particle emissions were considered in the model. Based on the model simulation by Xian et al. (2013) that considers non-smoke aerosol sources, we expect that the maximum contribution from non-smoke AOD on average should be ~ 0.1 in our study.

Higher TOA shortwave direct radiative forcing (SWDRF) (Fig. 1e) induced by smoke aerosol particles mainly occur over areas previously mentioned that are associated with high smoke AOD, and where the positive value of SWDRF may be larger than $15\,\mathrm{W\,m^{-2}}$. The SWDRF here is the net downward SW flux difference at TOA between the simulation that considers smoke radiative effect and the simulation that does not consider it (similar to the definition in Zhao et al., 2010). There is a higher contrast, as well as spatial discontinuity, in

SWDRF between land and ocean than that of AOD. Larger values are not only over the land with high smoke emission, but also over the ocean southwest of Sumatra (Fig. 1e). The positive forcing at the TOA can be understood through two factors: (a) the single-scattering albedo of smoke particles, which is about 0.8 (based upon AOD and AAOD shown in Fig. 1) and which governs the portion of solar energy that is lost in the atmosphere due to absorption by the smoke particles; and (b) the underlying surface or cloud properties of the aerosol layer that regulates the amount of solar energy being re-directed, through reflection or multi-scattering, for the smoke particles to either absorb or reflect (Hansen et al., 1997). Detailed analysis shows that (b) is a dominate factor in our study region because (i) in October boundary clouds are generally persistent throughout the region, particularly in the west Sumatran Low (Reid et al., 2012, 2013); (ii) neither the distribution of AOD (with high spatial variation from 0.1 to 1.1, Fig. 1a) nor the absorption of aerosol optical depth (AAOD with small spatial variation from 0.17 to 0.20, Fig. 1b) over the 8° S–0° zone reflect the land–ocean discontinuity of SWDRF; (iii) large positive SWDRF are in the locations where outgoing shortwave flux (O-SW) at the TOA is also high (Fig. 1d) due to a large cloud fraction; and (iv) the discontinuity (e.g., less than $60\,\mathrm{W\,m^{-2}}$) of outgoing shortwaves at TOA between the land and sea reflects the impact of sea breezes (Wang et al., 2013) and the resultant low-cloud fraction during daytime along the coast. Similar results were found over the Amazon region during the dry season (Koren et al., 2004), where satellite data showed that scattered cumulus cloud cover was reduced by smoke particles, and this response can reverse the regional smoke instantaneous forcing of climate from $-28\,\mathrm{W\,m^{-2}}$ in cloud-free conditions to $8\,\mathrm{W\,m^{-2}}$.

The analysis of the vertical profile of smoke aerosols and clouds over the smoke source region during this month in Wang et al. (2013) showed that a significant amount of smoke particles are within and above the low-level cloud layer (see the later discussion of Fig. 6). To further confirm that the warming at the TOA is due to aerosol particles both above and mixing with the cloud, we also analyzed the SWDRF in clear-sky conditions (average SWDRF when the cloud fraction of less than 0.05, Fig. 1f) and found a strong negative forcing of up to $-20\,\mathrm{W\,m^{-2}}$. This also partially explains some of the negative forcing in all-sky conditions such as in the area around Borneo Island that has a lesser cloud fraction. By restricting the analysis of SWDRF at TOA in conditions of a cloud fraction less than 0.05 respectively for low-level clouds, mid-level clouds, and high-level clouds only (Fig. S1a–c), we found that SWDRF with a low-level cloud fraction of less than 0.05 (Fig. S1a) is very similar to that in conditions with a column cloud fraction of less than 0.05 (Fig. 1f). SWDRFs for both middle-level and high-level cloud fractions less than 0.05 are similar in all-sky conditions. The above analysis suggests that low-level clouds play a more important role than mid-level and high-level clouds in causing the positive forcing of smoke aerosols.

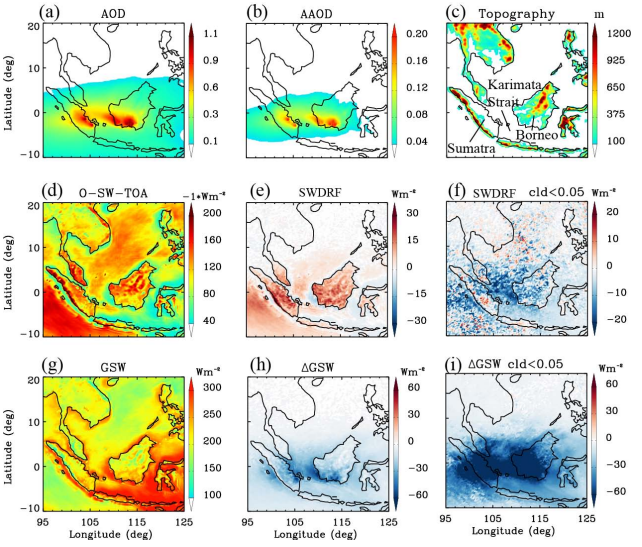

Fig. 1. Distribution of monthly averaged variables in October 2006. **(a)** aerosol optical depth (AOD) in 600 nm, **(b)** aerosol absorption optical depth (AAOD) in 600 nm, **(c)** topography in meters, **(d)** outgoing shortwave (SW) at top of amosphere (TOA), O-SW-TOA, **(e)** aerosol shortwave direct radiative forcing (SWDRF) at TOA, **(f)** aerosols SWDRF at TOA for column cloud fraction less than 0.05, **(g)** net shortwave flux at the ground (GSW), **(h)** difference of GSW (ΔGSW), **(i)** ΔGSW for column cloud fraction less than 0.05. The difference of each variable (ΔV) is defined as $\Delta V = V_{\mathrm{Ra}} - V_{\mathrm{non\text{-}Ra}}$. The OC / BC ratio is 10 in the simulation.

As a result of the extinction of solar radiative flux by smoke particles in the atmosphere, the net shortwave flux at surface or ground (GSW) is reduced (Fig. 1h). Large reductions are in regions where the cloud fraction (as indicated by the outgoing shortwave at TOA, Fig. 1d) is low and AOD (Fig. 1a) is relatively high. As much as $60\,\mathrm{W\,m^{-2}}$ of GSW is reduced in the Kalimantan region and in the area of the Karimata Strait nearest to Kalimantan, and $\sim 30\,\mathrm{W\,m^{-2}}$ of reduction occurs in the downwind ocean region, which respectively corresponds to $\sim 20\,\%$ and $10\,\%$ of the net solar input (or GSW) at the surface (Fig. 1g). The distribution of GSW (Fig. 1g) generally exhibits an opposite pattern to that of the outgoing shortwave at TOA (Fig. 1d), showing larger values (an increase of $\sim 100\,\mathrm{W\,m^{-2}}$ compared to that over land) along the coastal ocean due to the sea-breeze-induced small cloud fraction. Analysis of the change of GSW (ΔGSW) by smoke particles in clear-sky conditions (with a cloud fraction less than 0.05, Fig. 1i) shows a much larger reduction of GSW than the counterparts in all-sky conditions, especially over the smoke source region (the area where the monthly averaged AOD is larger than 0.5 in Fig. 1a); this difference again underscores the importance of a relative vertical position between aerosols and clouds in estimating all-sky aerosol radiative effects.

With a climate model at a spatial resolution of 3.75° longitude by 2.5° latitude, Davison et al. (2004) estimated the smoke radiative forcing at the surface which resulted from the Indonesian forest fires in September 1997 to be $\sim 200\,\mathrm{W\,m^{-2}}$ or a 75 % reduction of the total incident SW flux. The difference between our estimate and that in Davison et al. (2004) may in part be due to the difference in smoke emission. The smoke emission in September–October 2006 is estimated as ~ 3.48 Tg after the doubling of FLAMBE's emission (Wang et al., 2013) and thus is much lower than 26.07 Tg for the same two months in 1997 (Davison et al., 2004), although both estimates bear uncertainty by a factor of 2 (Reid et al., 2013).

A further detailed contrast of Fig. 1c with Fig. 1h reveals the impact of topography on the smoke transport and its associated radiative effects. Simulated at a spatial resolution of 27 km, the results show a very minimal effect of smoke on GSW over the Barisan mountain range along the western side of Sumatra Island and the Tama Abu Mountain that covers half of north Borneo Island. Due to the obstruction of the Barisan range, the smoke transport pathway under southerly trade winds bifurcates into two branches confined respectively at the eastern and western sides of the Barisan range, leading to a divergence of smoke concentration and consequently a smaller reduction of GSW over the mountainous area. In fact, the spatial distribution of both simulated an outgoing shortwave radiation (Fig. 1d) and GSW (Fig. 1g), and reflected the influence of topography and land use change. Regions with high (low) elevation generally have low (high) surface albedo and hence larger (lower) GSW and less (more) outgoing shortwave radiation. Such fine-scale topography-related features of the radiative transfer calculation are not manifested in the results by Davison et al. (2004) and Ott et al. (2010) from coarser-resolution model simulations, and, consequently, the aerosol loading and smoke forcing over the Indian ocean shown in their studies may have an overestimation as the mountain's blocking of smoke transport is not well resolved in the model. A similar kind of overestimation can be found in Duncan (2003), in which the transport of smoke particles from the 1997 Indonesian wildfire events is simulated with a GEOS-Chem model (Goddard Earth Observing System) at 2.5° longitude by 2° latitude horizontal resolution.

In response to a smoke-induced change of radiation at both the surface and TOA, the change of surface energy budget and the surface temperature is quite large as depicted in Fig. 2. Over the land region, both sensible heat (SH, Fig. 2a) and latent heat (LH, Fig. 2c) show a south–north gradient, with highest SH and lowest LH, respectively, in the south. The pattern of SH is consistent with the spatial distribution of GSW and also 2 m temperature ($T2$) (Fig. 2e). Generally, fewer clouds lead to more downward GSW radiation and hence higher $T2$. Higher SH can be found in the southern part of Kalimantan, the southeastern region of Sumatra, and Java southern Sulawesi (Fig. 2a). The pattern of LH more or less reflects the availability of water at the surface and the surface wind speed (Fig. 5a and c), with both having higher values over the ocean than over land. Due to less availability of soil moisture and precipitation at land area south of 2° S (Fig. 3c), LH there is lower compared to the northern land region. The partition of net radiative energy at the surface in the form of SH is smaller than that in the form of LH excepting the land region south of 2° S, which is consistent with the Bowen ratio (ratio of sensible to latent heat) distribution with values of ~ 0.05 over ocean, ~ 0.5 over land area, ~ 0.2 for tropical forests and $\sim$ 1–10 in dry land to deserts (Stull, 2000).

As a result of the reduction of GSW, both sensible heat flux at the surface (SH) (Fig. 2b) and latent heat (LH) (Fig. 2d) are decreased by up to $20\,\mathrm{W\,m^{-2}}$ in the Kalimantan and Sumatran regions. The large reduction of both SH and LH is confined mainly over the land, particularly in the smoke source region (Fig. 2b and d), while no evident change of SH and LH can be found over the ocean. Similarly, the change of $T2$ ($\Delta T2$) as a result of the smoke radiative interaction is more significant over land than over open oceans that have a much larger heat capacity and latent heat release (Levitus et al., 2012). Note that since WRF-Chem does not have a multi-layer ocean model, simulated here for the ocean is the bulk sea surface temperature rather than the sea surface skin temperature. When compared to the land surface temperature, the monthly mean of sea surface temperature generally shows much less variation and is more regulated by the oceanic currents and deep mixing that are not simulated in the WRF-Chem. Hence, the changes of SH and LH due to the smoke radiative effect are restricted to the land (as shown in Fig. 2b and d), which is also consistent with Wang and Christopher (2006).

Because of the large reduction of GSW at the surface, $T2$ decreases by up to 1 K and 0.5 K, respectively, during daytime (between 08:00 LT and 19:00 LT) over the Kalimantan and Sumatran regions that have a high loading of smoke aerosols (Fig. 2f). This decrease also has a residual effect at night, leading to a decrease in night temperature by 0.1 K in both regions (Fig. 2h). In contrast, because of the enhanced heating ($\sim$ 2–3 $\mathrm{K\,day^{-1}}$ during noon, Fig. 6e) due to the absorption of solar radiation by smoke particles, T at 2200 m above the surface increases by up to 0.6 K and 0.2 K, respectively, during the daytime in the Kalimantan and Sumatra regions (Fig. 2j). However, this increase has nearly a zero residual effect at night (Fig. 2l). Note that the model captures well the higher $T2$ over land (except regions with high topography) and lower $T2$ over the ocean during daytime (Fig. 2e). The opposite contrast happens during the nighttime (Fig. 2g). However, neither such day-to-night contrasts nor land-to-ocean contrasts are seen at 2200 m above the surface, reflecting the low boundary layer height in this region (Wang et al., 2013), and the efficient mixing of heat in the atmosphere above the planetary boundary layer height (PBLH).

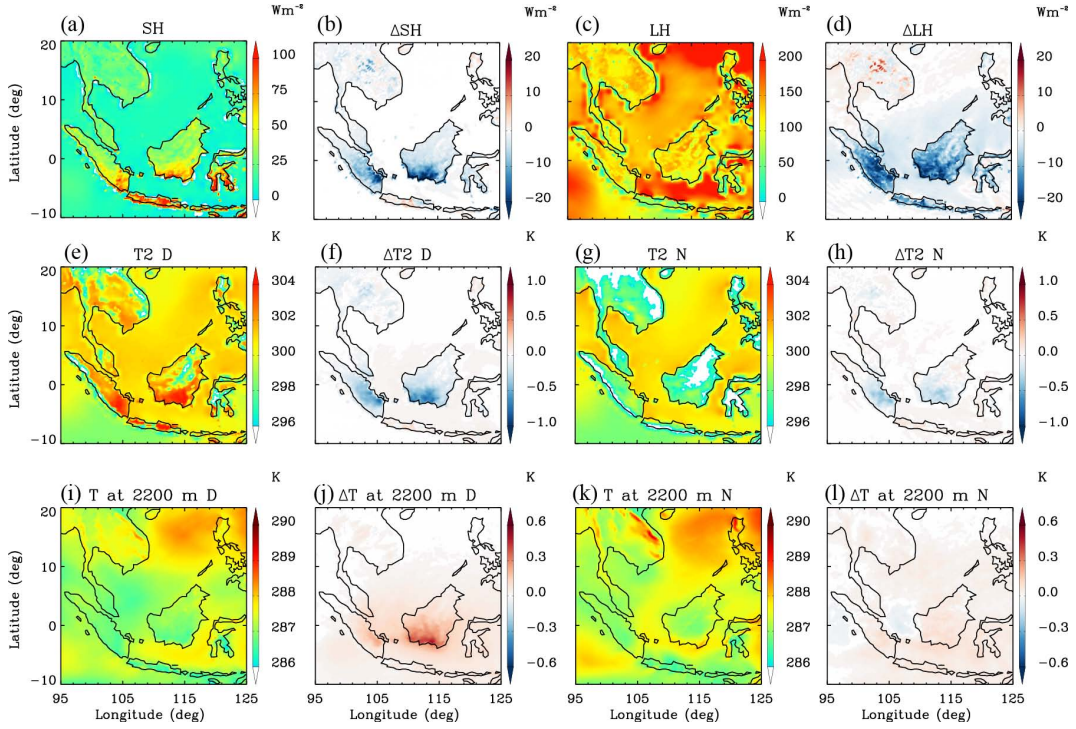

Fig. 2. Distribution of monthly averaged variables in October 2006. **(a)** Sensible heat flux at the surface (SH) without consideration of smoke radiative interaction, **(b)** difference of SH (ΔSH) due to the smoke radiative interaction. **(c–l)** are all paired similarly to the pair of **(a)** and **(b)** but for latent heat (LH), 2 m air temperature ($T2$) at daytime, $T2$ at night, temperature at 2.2 km above terrain at daytime, and temperature at 2.2 km above terrain at nighttime, respectively. The difference of each variable (ΔV) is defined as $\Delta V = V_{\mathrm{Ra}} - V_{\mathrm{non\text{-}Ra}}$. D donates daytime, i.e., the time period between 08:00 LT and 19:00 LT, and N donates nighttime, i.e., between 20:00 LT and 07:00 LT. The OC / BC ratio is 10.

3.2 Smoke radiative effect on boundary layer processes

To a large extent, the distribution of the PBLH (Fig. 3a) resembles that of SH and $T2$ (Fig. 2a and e) and is opposite to that of cloud cover as indicated in the outgoing shortwave in Fig. 1d. With less cloud cover and warmer land surface, the PBLH on average is higher over the two smoke source regions of south Sumatra and south Kalimantan (Fig. 3a). Also, the nearby ocean of south Kalimantan has high PBLH due to less cloud cover and a warmer surface. In response to the decrease of surface temperature and the increase of the heating rate in the atmosphere due to smoke absorption, the atmospheric stability is increased in the lower troposphere, and the turbulent mixing process within the PBL is decreased. This consequently results in a reduction of PBLH up to 120 m (or ∼ 10 %) over Sumatra and the Kalimantan region in monthly averages (24 h) (Fig. 3b). The distribution of this reduction is similar to the change of SH (Fig. 2b) with minimal values over the ocean. Although more stability is introduced to the PBL by the smoke aerosol over the fire area and the most downwind region, the regions over a narrow belt of the Karimata Strait and the south coastal ocean of the Kalimantan PBL seem unstable (Fig. 3b). The reason for this will be explored further in Sect. 3.3.

Figure 3c and d show the distribution of precipitable water and its change due to smoke radiative impact. October is a transition time for ITCZ moving southward, and from the distribution of precipitable water we can see the distinct line at ∼ 1° S between the wet region at the north and the dry area at the south. When considering the smoke aerosols' radiative interaction, the increase of precipitable water occurs over the fire area and the most downwind region, and a larger increase occurs over the Karimata Strait.

To reveal the dynamical processes that contribute to the change of PBLH as a result of smoke radiative interaction, Fig. 4 shows a vertical cross section centered at the latitude of 1° S (extends 2 grid points into and out) that passes through the densest smoke of the smoke source region. Included are monthly averages of $PM_{2.5}$ mass concentration, PBLH simulated with the radiative effect of smoke aerosols (solid line) and PBLH simulated with (solid line) and without (dotted line) the radiative effect of smoke, as well as the differences of temperature (ΔT) and precipitable water (ΔPW). The response of air temperature to the smoke radiative heating in the atmosphere and radiative cooling near the surface depends highly on the aerosol vertical profile that also has an important diurnal variation as a result of the boundary layer process (Wang and Christopher, 2006 _ENREF_19). Because of the dominant subsidence in the upper troposphere

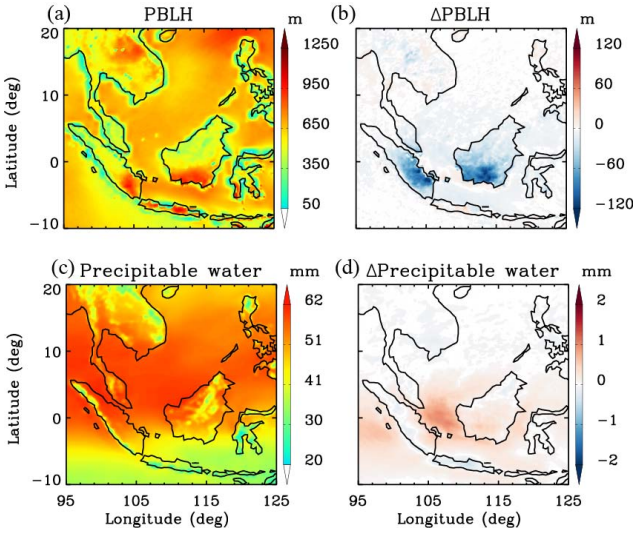

Fig. 3. Distribution of monthly averaged variables in October 2006. **(a)** Planetary boundary layer height (PBLH) without considering the radiative effect of smoke aerosols, **(b)** difference of PBLH due to the radiative effect of smoke aerosols. **(c)** and **(d)** are respectively same as **(a)** and **(b)** but for precipitable water. The OC / BC ratio is 10 in the simulation.

over the smoke source region (Fig. 4a; also Wang et al., 2013), the transport of smoke particles to the middle atmosphere is suppressed, and a high concentration of smoke particles can be found around 2–3 km above the boundary layer (Fig. 4a). Note that this smoke layer may not be well characterized by CALIOP because of the co-existence of cloud layer and overlying cirrus clouds (Wang et al., 2013). Nevertheless, this layer is very distinct from the boundary layer during the morning when boundary layer convection has not been well developed (Fig. 4a). Correspondingly, during the morning (10:00 LT), an increase of air temperature by up to 0.3 K can be clearly seen at 1–3 km altitude (Fig. 4c), which is above the boundary layer over the smoke source region.

As time progresses to the late afternoon (17:00 LT) when the convective boundary layer is well developed, the smoke particles are not only well mixed within the boundary layer, but also are transported and mixed with the particles that already exist at 1–3 km from the previous smoke emission (Fig. 4e). Indeed, the contrast between Fig. 4a and e shows that the subsidence is much weaker in the middle troposphere ($\sim$ 3–6 km) in the late afternoon as compared to the morning, which is favorable for the vertical transport of smoke particles from the boundary layer to the middle troposphere. A corresponding increase of air temperature by 0.6 K can be seen over the smoke source region and by $\sim$ 0.1–0.4 K over nearby ocean at an altitude of 3–6 km (Fig. 4g). During the night, however, PBLH is lower, and a residual layer with high smoke aerosols between 1 and 2.5 km is decoupled from the nocturnal boundary layer (Fig. 4i). This decoupling is also associated with the shift of upward motion to the downward motion around 1 km at night (Fig. 4i). The temperature change during night is essentially a residual effect from daytime (Fig. 4k).

As discussed in Sect. 3.1, the air temperature change (ΔT) due to smoke particles in the boundary layer is more complex because the warming due to smoke absorption can be overwhelmed by the cooling from the surface through turbulent mixing. Indeed, Fig. 4c and g show that cooling occurs nearly everywhere in the boundary layer, but only over the smoke source region, regardless of the time of day. During the morning, when the elevated smoke layer is lying above the PBLH and there is not much smoke aerosol below 1 km above the surface, the radiative extinction contributed by the elevated smoke layer leads to a strong cooling within the PBL. During late afternoon, the increase of smoke aerosols induces strongest warming in mid-altitude. And within the PBL smoke aerosols induce both warming (through absorbing) and cooling (through scattering); overall the cooling effect overwhelmed but much weaker compared with that during morning time.

It should be noted that dynamics and radiative effects are coupled; the warming by smoke particles confined over the smoke source region in the morning (10:00 LT) can produce an updraft above the PBLH (Fig. 4b). Then the updraft in lower troposphere combined with the overwhelming downdraft in the upper troposphere (Fig. 4a) further result in a local convergence around the altitude of 2–3 km. Also the updraft in mid-altitude would transport more smoke particles from the PBL, and thus constitutes a positive feedback on smoke concentration above the boundary layer. This hypothesis is supported by the following model results: (a) in the morning (10:00 LT) the smoke radiative effects result in an increase in smoke concentration by $\sim 4\,\mu g\,m^{-3}$ over 2–3.5 km and a similar decrease between 1 and 2 km, suggesting a local convergence at 1–2 km above surface; (b) such an increase of $PM_{2.5}$ at 2–3.5 km and a decrease between 1 and 2 km are even stronger up to $10\,\mu g\,m^{-3}$ in the later afternoon (17:00 LT), suggesting an enhancement due to the positive effect.

To illustrate the change of surface $PM_{2.5}$ introduced by smoke, we used one of the smoke source regions, Borneo Island (the location of Borneo Island can be seen in Fig. 1c) as an example. Borneo Island experienced a distinct alternation of sea breeze and land breeze (Wang et al., 2013). Sea breeze is very strong in the afternoon (Fig. 5a), and land breeze is prominent at midnight (Fig. 5c). When aerosol radiative interaction is considered, sea breeze (Fig. 5a) (or land breeze (Fig. 5c)) at daytime (or nighttime) along the south coastal line of Borneo is weakened (or strengthened) up to $0.3\,ms^{-1}$. At daytime, due to the weakened sea breeze, a surface convergence occurs over the southern part of Borneo, and the decrease of smoke aerosols up to $2\,\mu g\,m^{-3}$ can be found there

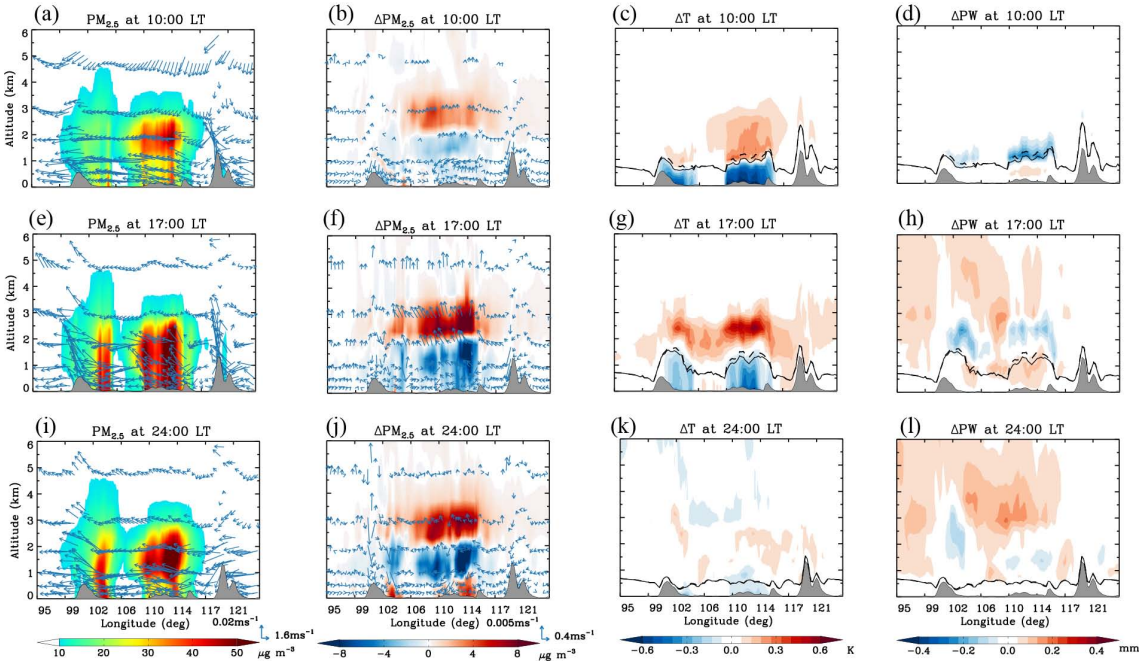

Fig. 4. Top row: vertical cross section of monthly averaged variables in October 2006 at 10:00 LT for **(a)** $PM_{2.5}$ and u-w wind speed; **(b)** change of $PM_{2.5}$, $\Delta PM_{2.5}$; **(c)** change of temperature, ΔT; and **(d)** change of precipitable water, ΔPW. Second and third row are the same as the top row but at 17:00 LT and 24:00 LT, respectively. All variables are averaged along the vertical cross section centered at the latitude of 1° S (extends 2 grid points into and out). The terrain is also shown as gray shading in each panel. The difference of each variable (ΔV) is defined as $\Delta V = V_{Ra} - V_{non\text{-}Ra}$. The OC / BC ratio is 10 in the simulation. Also overlaid in some panels are the PBLH simulated with the radiative effect of smoke aerosols (black line) and PBLH without the radiative effect of fires (dotted line).

(Fig. 5b). At nighttime a divergence occurs over the southern part of Borneo induced by the strengthened land breeze, and the increase of smoke aerosols can be up to 5 μg m^{-3} at nighttime (Fig. 5d). To summarize, the smoke aerosols can cause significant change in the wind circulation at different scales, both vertically and horizontally, and all these changes can in turn modify the distribution of aerosols.

Unlike the smoke particles that are injected into the atmosphere through fire-produced thermal buoyancy, water vapor is added into the atmosphere through surface evaporation. Over the smoke source region where soil is dry compared to the ocean, a large part of the water vapor is from ocean brought by the sea breeze (Fig. 3c). The smoke radiative effect results in reduction of PBLH and the more stable PBL; hence more water vapor is trapped in the PBL, which in turn leads to a lesser water vapor amount above the PBL in the morning (Fig. 4d). The perturbation of entrainment of drying could be another reason for the change in water vapor. Over the fire area during daytime (Fig. 4d and h), decreased PBLH can reduce the entrainment drying and increase PW within the PBL. Right above PBLH (about 1 km), because the warmer air induces a slight updraft, the entrainment of drying could be enhanced and so PW would be decreased. This is consistent with the simulations by Yu et al. (2002) of strongly absorbing aerosols above the PBL. When the smoke aerosol became more absorbing (with OC / BC as 3.5), such perturbation of PW within or above PBLH during the daytime became more prominent as shown in Fig. S2a and b. As time progressed toward afternoon, such a dichotomy was further amplified, with more water vapor trapped in the PBL and less water vapor above the PBL (Fig. 4h). The less water vapor above the PBL is further exacerbated by the updraft associated with the local convergence due to the smoke heating, and hence more water vapor can be seen between 3 and 6 km. The change in water vapor during nighttime (Fig. 4l) nevertheless can be considered as a residual effect from the day. Over ocean (106–110° E), the aerosol radiative interaction yields more low-level convergence (Fig. 4f) and a slightly unstable PBL structure (Fig. 3b), which will also be illustrated in Fig. 7 of Sect. 3.3. Since there is no shortage of water over an ocean, the resultant low-level convergence can transport more water vapor upward. Hence, on a monthly basis this may result in an overall increase of precipitable water over the Karimata Strait (Fig. 3d).

To focus on the area with maximum emissions, the monthly averaged vertical profiles of $PM_{2.5}$ concentration, heating rate, temperature and also their changes due to the smoke radiative interaction averaged for all grid boxes over the smoke source region at four different times are represented in Fig. 6. The surface smoke concentration was at a minimum in the morning (08:00 LT). The column burden of smoke mass increases rapidly after the fire activity starts

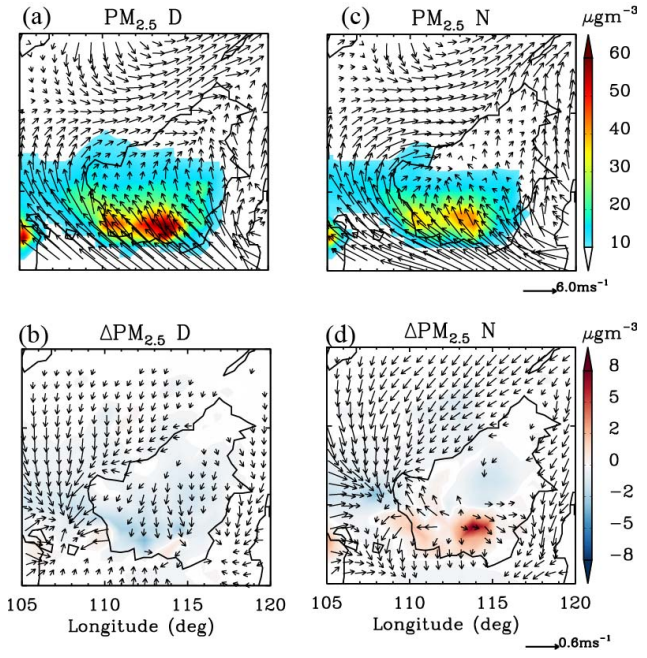

Fig. 5. Distribution of monthly averaged variables in October 2006. Anomaly of surface wind and monthly averages of surface $PM_{2.5}$ respectively at **(a)** daytime and **(c)** nighttime. Difference of surface wind anomaly and surface $PM_{2.5}$ in monthly averages due to smoke radiative effect at **(b)** daytime and **(d)** nighttime. The anomaly of surface wind is the difference between the wind at certain local time and the wind of monthly mean. The OC / BC ratio is 10 in the simulation.

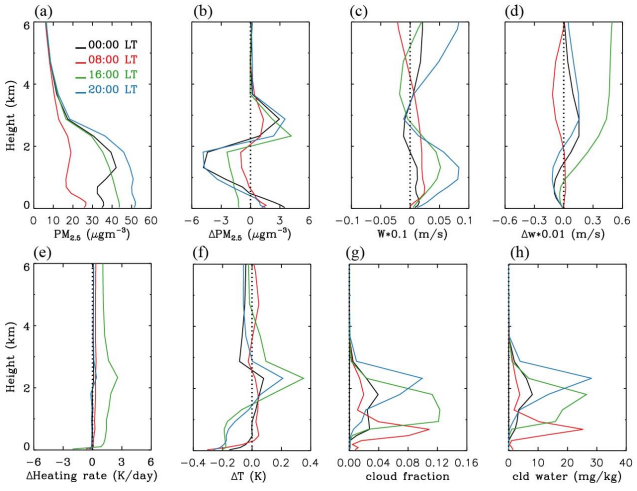

Fig. 6. Vertical distribution of monthly/domain averaged variables over the smoke source region in October 2006 at different local times for **(a)** $PM_{2.5}$ concentration, **(b)** difference of $PM_{2.5}$ concentration ($\Delta PM_{2.5}$), **(c)** vertical velocity (w), **(d)** difference of w (Δw), **(e)** difference of heating rate, **(f)** difference of air temperature (ΔT), **(g)** cloud fraction, and **(h)** cloud water. The difference of each variable (ΔV) is defined as $\Delta V = V_{\mathrm{Ra}} - V_{\mathrm{non\text{-}Ra}}$. The OC / BC ratio is 10 in the simulation. The smoke source region is the area where the monthly averaged AOD is larger than 0.5 (Fig. 1a).

in the morning (08:00 LT) and achieves maximum values in the early night (20:00 LT) (Fig. 6a). As PBL progresses from morning toward nighttime, with stronger turbulence mixing (and upward motion, Fig. 6c) together with the more intensified fire activities, a well-mixed vertical smoke distribution can be found at 16:00 and 20:00 LT within 2 km. The residue effect of smoke concentrations (00:00 LT) is obvious in nighttime within the whole column and more prominent at around 1.5 km. Consistent with our interpretation in Fig. 4, the increase of temperature (ΔT) induced by smoke particles is generally found to be between 1.5 and 3 km with a peak around 2 km (Fig. 6e), which leads to an increase of upward motion at this altitude range and to more stability (or overall slight decrease of upward motion) below this altitude (Fig. 6d). Consequently, the increase of $PM_{2.5}$ is found at 2–3.5 km with a peak around 3 km (Fig. 6b); the decrease of $PM_{2.5}$ and T due to the smoke radiative effect is found mainly below 2 and 1.5 km, respectively, during daytime. The staggering feature supports the hypothesis of the secondary circulation, e.g., an updraft above the boundary layer, introduced by the smoke absorption, as supported by the wind vector change in Fig. 4, although large-eddy simulations at a finer scale are needed to further test this hypothesis.

It is worth noting that within ∼200–300 m above the surface, $PM_{2.5}$ concentration is increased in the morning and night, with a larger increase during the night (20:00 LT). As discussed above (Fig. 4), different from at other times, at 16:00 LT the $PM_{2.5}$ decreases all the way below 2 km. In the morning (08:00 LT), the near-surface ΔHeating rate is negative with a small magnitude ($-0.5\,\mathrm{K\,day^{-1}}$), and at about 100 m above the surface ΔHeating rate turns to positive with $0.2\,\mathrm{K\,day^{-1}}$ (Fig. 6e). At 16:00 LT the ΔHeating rate is $-2\,\mathrm{K\,day^{-1}}$ near the surface, and above the surface it increases from less warming to the peak value which is near $6\,\mathrm{K\,day^{-1}}$ at ∼2.5 km. The response of ΔT to the ΔHeating rate involves the heat transfer through turbulent mixing within the PBL. At 00:00 LT, ΔT is negative with a small magnitude (0.15 K) that appears near the surface due to the residual effect of ΔT in the daytime. In the morning (08:00 LT) as the sun rises, the ΔT is more negative (cooler) near the surface and becomes positive (warming) at ∼500 m. In the afternoon, in association with the stronger mixing, the critical layer at which the ΔT shifts from negative to positive is near 2 km at 16:00 and 20:00 LT.

An analysis of a case study during a heavy smoke event (Fig. S4) and also for several other big events in October 2006 (Fig. S6) shows that the aerosol radiative impacts are more prominent compared to the monthly averaged effects. For the afternoon time during a heavy smoke event during 12:00–16:00 LT on 31 October 2006, the positive value of SWDRF can be up to $60\,\mathrm{W\,m^{-2}}$ over downwind area

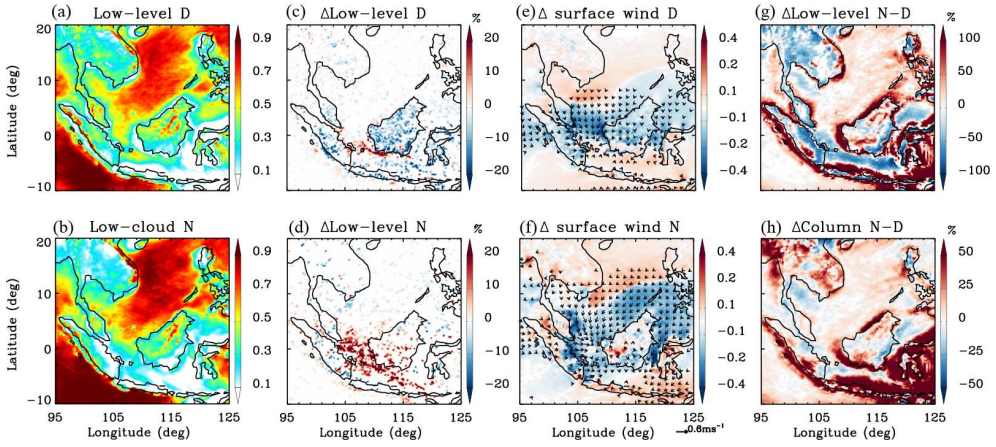

Fig. 7. Distribution of monthly averaged variables in October 2006. **(a)**, **(c)** and **(e)** in top row are simulated for daytime **(a)** low-level cloud fraction, **(c)** the differences of low-level cloud fraction, and **(e)** the differences of surface wind speed. **(b)**, **(d)** and **(f)** are same as **(a)**, **(c)** and **(e)** but for nighttime. **(g)** is the difference between **(d)** and **(c)**; **(h)** is the difference of column cloud between nighttime and daytime. All the difference showed here with 95 % confidence by paired samples t test. Clouds below 2000 m are considered low-level clouds. Note in panel **(e)** and **(f)** the color-filled contours represent the wind speed. The OC / BC ratio is 10 in the simulation.

(Fig. S4f) with high AOD (higher than 2.5) and AAOD (around 0.5) over Borneo Island. The GSW can be decreased by 400 W m^{-2} from 800 W m^{-2} (Fig. S4g), and the resultant reduction of $T2$ and PBLH can reach up to 2 K (from 304 K) and 800 m (from 1600 m), respectively; T increases at 2200 m (Fig. S4i) can be 2 K (much lager than the monthly average value of 0.6 K). Over most the downwind area at Borneo Island the low-level cloud fraction during afternoon time is decreased by 40 % in the simulation (Fig. S4o).

3.3 Cloud

Over the Southeast Asian Maritime Continent, cloud cover (Fig. 7a and b) is persistent during both day (denoted as D) and night (denoted as N). This large cloud cover is primarily contributed by the high-level clouds (6000 m above surface, Fig. S3c and g), although the fraction of low-level clouds (2000 m above surface) is also important, with a monthly average of 0.6 over ocean and 0.25 over land (Fig. 7a and b). The mid-level cloud fraction over both land area and ocean region is generally below 0.1 (Fig. S3b and f). Because of this small amount of middle-level clouds and also because smoke is seldom transported to above 6 km to alter the high-level cloud fraction in any radiatively discernable quantity, our analysis focused on the change in low-level clouds (ΔCloud $= \text{Cloud}_{\text{Ra}} - \text{Cloud}_{\text{non-Ra}}$) due to the smoke radiative effect. Indeed, the change in low-level clouds (Fig. 7c and d) is representative of the change of columnar cloud cover in both day and night (Fig. d and S3h). We noticed that the change of cloud was contributed to by the semi-direct effect and did not include the influence of an indirect effect since the indirect effect is turned off in all the simulations and is thought to be relatively very small over MC in this particular strong biomass burning period.

Over the Malay Peninsula, Sumatra Island and Borneo Island, the low-level cloud fraction during daytime is decreased by more than 10 % in the simulation (Fig. 7c) due likely to the smoke-induced reduction of evaporation at the surface (Fig. 2d), the increase of atmospheric stability in the boundary layer (Fig. 3b), and the increase of the solar heating rate around 2 km (Fig. 6c), all of which are discussed in the previous section. The change in cloud fraction is consistent with past studies. For example, the dominant effect of the aerosols to reduce clouds and precipitation in the afternoon was found in Wu et al. (2011a, b) when they studied the biomass burning event in the dry season of South America. Koren et al. (2004) reported that scattered cumulus cloud cover over the Amazon region can be reduced by 38 % due to smoke semi-direct effects. Zhang et al. (2008) did ensemble simulations about the impact of biomass burning aerosol on land–atmosphere interactions over the Amazon, and found cloudiness decreases in early afternoon due to the absorption of solar radiation by smoke aerosols. However, what is unexpected is an increase of cloud cover over a narrow belt region of the Karimata Strait and the south coastal ocean of Kalimantan (Fig. 7c). Compared to the daytime, a distinct difference in the nighttime is the increase of cloud fraction over most areas of the the Karimata Strait and the Java Sea (Fig. 7d), and virtually no decrease of cloud fraction in heavy smoke regions. The increase of cloud fraction in both daytime and nighttime can be attributed to the change of the low-level wind pattern ($\Delta\text{Wind} = \text{Wind}_{\text{Ra}} - \text{Wind}_{\text{non-Ra}}$) (Fig. 7e and f). During daytime, the southeast trade winds increase over most regions south of -1° S (the red shaded area in Fig. 7e), and decrease after crossing the Equator (the blue shaded area in Fig. 7e). Consequently, a dynamic low-level convergence is formed over the Karimata Strait and the south

coast of Kalimantan, favoring the low-level cloud formation. In contrast, during nighttime, a larger area with more convergence and hence increased formation of clouds (Fig. 7f) can be seen over both the Karimata Strait and the Java Sea.

The contrast of the changes of cloud cover due to the smoke radiative effect between night and day, and between the ocean and land, reflects the importance of considering the surface properties. Over land, smoke semi-direct effect is important in daytime as it increases stability and the saturation of water vapor pressure through the heating within clouds (Fig. 6f), reducing the cloud cover. However, there is virtually a zero effect at night. Over most ocean areas, the smoke semi-direct effect is much less. The large day–night difference of columnar cloud fraction due to a smoke radiative effect is mainly located in the coastal regions (Fig. 7g), and is primarily contributed by the change in the low-level cloud fraction (Fig. 7h). This suggests that the change of sea breeze likely plays a role in changing the cloud fraction by extending the offshore convergence zone; the daytime decrease (increase) of low-level (middle-level) air temperature over land weakens the sea breeze, while the nighttime decrease of surface temperature over the land enhances the land breeze.

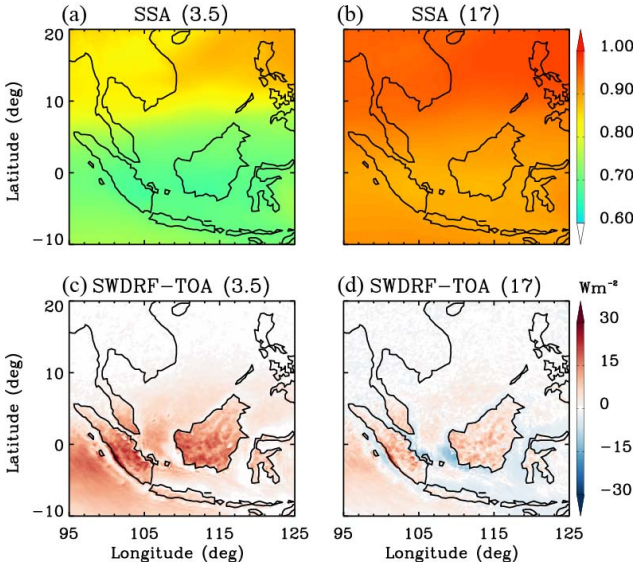

Fig. 8. Distribution of monthly averaged variables in October 2006 for **(a)** single-scattering albedo (SSA) in 600 nm, **(c)** SWDRF with OC / BC ratio 3.5, **(b)** and **(d)** are same as **(a)** and **(c)** but with OC / BC ratio 17.

4 Sensitivity experiments to the OC / BC ratio

By conducting a sensitivity experiment with respect to the change of OC / BC ratio, we can re-examine the processes relative to smoke particle absorption. When the OC / BC ratio changed from a smaller to a larger value, the total mass of OC and BC is unchanged, meaning scattering aerosols increased and absorbing aerosols decreased. Processes should respond differently to the change in smoke absorption and also the resultant change of atmospheric temperature profile. When the OC / BC ratio was changed from 3.5 to 17, the average SSA over Kalimantan and Borneo changed from roughly 0.65 to 0.9 (Fig. 8a and b). A change in the OC / BC ratio from 10 in a base case to 3.5 (17) results in a factor of 2 increase (decrease) in the SWDRF (Fig. 8). A smaller OC / BC ratio leads to more warming in the atmosphere, while increases of the OC / BC ratio lead to more cooling at the surface. Indeed, SWDRF is negative over the east part of Karimata Strait for the cases with an OC / BC ratio of 17, and close to zero over most land regions. Hence, Fig. 8 verifies that the positive SWDRF in baseline cases is due to the absorptive smoke particles within and above the low-level clouds. As mentioned in previous sections, over a smoke source region, the CCN concentration likely has a saturated association with convective clouds. The indirect effects are not considered in this study. While the indirect effects might become critically important over the area further out from the MC.

To summarize, averaged quantities with different OC / BC ratios in October 2006 over the smoke source region are shown in Fig. 9a. Overall, for the variations of OC / BC ratio from 3.5 to 10, and to 17, AOD has the smallest changes (< 5 %), while other variables have a larger response especially when the OC / BC ratio changed from 3.5 to 10. A reduction of ∼ 20 % can be found for PBLH, $T2$, CLD, GSF, LH, SH, AAOD, and SWDRF when the OC / BC ratio is changed from 3.5 to 10. Interestingly, a net change of cloud fraction increases the ratio, and such an increase gets smaller as aerosols become more scattering (or as the OC / BC ratio gets larger). Analysis focusing separately on daytime versus nighttime shows that this overall increase in cloud fraction is due to the large increase in cloud fraction at night (Fig. 7d). What is shown in Fig. 9a can also be found for a big event on 31 October 2006 (Fig. 9b). The aerosol radiative impact of this big event is much more prominent compared to the monthly averaged impacts; detailed analysis can be seen in Sect. 5.

Figure 10 shows the 30-day averages of the vertical distribution of $PM_{2.5}$ concentrations, temperature (black line) and the difference (colored line) of each variable ($V = V_{\mathrm{Ra}} - V_{\mathrm{non\text{-}Ra}}$) caused by the radiative effect of smoke aerosol with varying OC / BC ratios averaged in the smoke source region in October. The change in $PM_{2.5}$ concentration and temperature shows a similar pattern for varying OC / BC ratios, and the higher concentration of BC always enhances the change. Most smoke aerosol can be found within 2 km above the surface. The aerosol mass increase near the surface is $\sim 1.5\,\mu g\,m^{-3}$ for OC / BC of 10 and 17, $\sim 2\,\mu g\,m^{-3}$ for OC / BC of 3.5. The decrease in $PM_{2.5}$ concentration occurs between 0.6 km and 2 km with a peak value of $-4\,\mu g\,m^{-3}$ (for OC / BC of 3.5), and $-2.5\,\mu g\,m^{-3}$ (for OC / BC of 10 and 17) at 1.5 km. Around 3 km above the surface, only a slight increase in $PM_{2.5}$ occurs for OC / BC of 17, and the

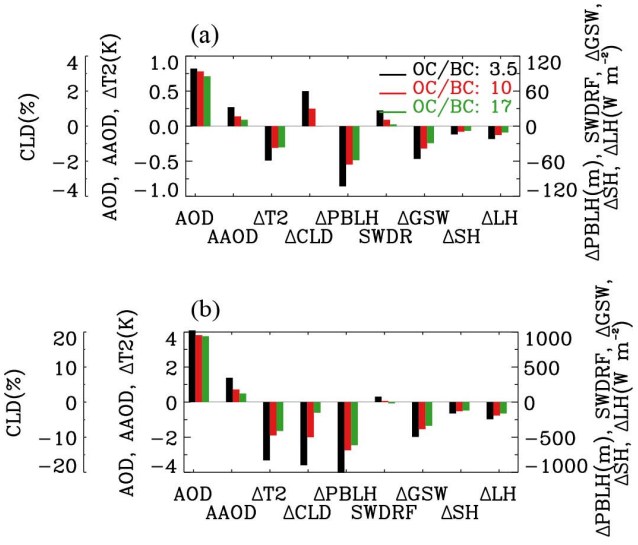

Fig. 9. (a) Monthly and domain averages over the smoke source region simulated with different OC / BC ratios in October of 2006 for AOD and AAOD, as well as the change of $T2$, CLD, PBLH, SWDRF, GSW, SH, and LH due to the consideration of smoke radiative effect. The change of each variable is defined as the difference between the simulation with and without the smoke aerosol radiative interaction ($\Delta V = V_{\mathrm{Ra}} - V_{\mathrm{non\text{-}Ra}}$). **(b)** same as **(a)** but for hourly averages of the daytime (08:00–17:00 LT) on 31 October 2006. (In the case of OC / BC as 3.5, 10 and 17, respectively).

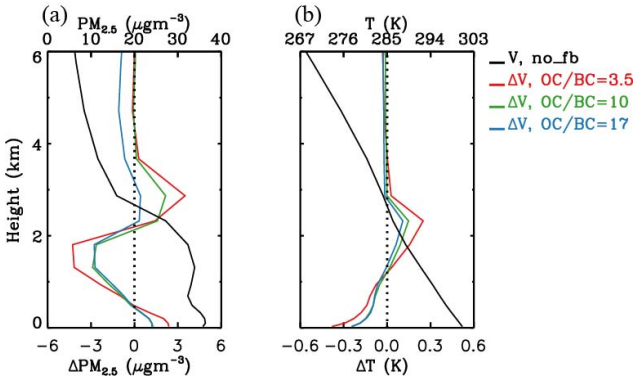

Fig. 10. Vertical distribution of monthly/domain averaged variables over the smoke source region in October 2006 for different OC / BC ratios: **(a)** $PM_{2.5}$ concentration, **(b)** air temperature. The black line is the variable (V), and the 3 other lines are the differences of the variable due to smoke ($\Delta V = V_{\mathrm{Ra}} - V_{\mathrm{non\text{-}Ra}}$) with different OC / BC ratio. (In the case of OC / BC are 3.5, 10 and 17, respectively).

peak value is 2.5 and 3.2 μg m^{-3} for OC / BC of 10 and 3.5, respectively. Air temperature increases above 1.2 km have a peak value of 0.3 K at 2 km for OC / BC of 3.5, and decreases below 1.2 km have a peak value of −0.4 K at the surface for an OC / BC value of 3.5. The change in air temperature for OC / BC of 17 and 10 is minimal, with a maximum decrease (−0.25 K) at the surface, and a maximum increase of 0.1 K at 2 km. Overall, stronger absorption leads to a more stable lower troposphere, along with the enhancement of aerosols above the PBL and near the surface, and the reduction of aerosols in the middle-to-upper fraction of the PBL.

5 Summary

The direct and semi-direct radiative impact of smoke particles over the Southeast Asian Maritime Continent (MC, 10° S–10° N, 90–150° E) during October 2006 were studied in the online-coupled Weather Research and Forecasting model with Chemistry (WRF-Chem). The unique vertical position between absorbing smoke particles and clouds led to a chain of interesting perturbations of boundary layer processes and of low-level cloud formations in the context of an already interesting meteorological regime that includes the sea breeze and trade winds. Due to a dearth in observation, we were not able to do a realistic comparison, so most results showed the possibilities only under the physical mechanism represented in the model. Key findings from this study can be summarized as the following:

1. Persistent and large low-level cloud cover in this region is found to enhance the net absorption of the surface/atmosphere with smoke particles within and above the low-level clouds. This results in a positive forcing of smoke particles at the top of the atmosphere, with a monthly and domain-averaged value of $\sim 20\,\mathrm{W\,m^{-2}}$ over Borneo and Sumatra and $\sim 60\,\mathrm{W\,m^{-2}}$ during the afternoon of 31 October over Borneo for an OC / BC ratio of 10.

2. The decrease of land surface temperature (up to 1 K for a monthly average and 2 K during the afternoon of 31 October) as a result of smoke radiative extinction of solar input leads to decreases in turbulence, and in the PBLH (100 m for monthly average and more than 800 m during the afternoon of 31 October), and to the weakening of the sea breeze. The aerosol-induced updrafts above BPL in turn favor an upward turbulent transport and thus lead to the increase of monthly smoke concentration by $\sim 4\,\mu\mathrm{g\,m^{-3}}$ (monthly afternoon time can increase $\sim 10\,\mu\mathrm{g\,m^{-3}}$) over 2–3.5 km. Surface $PM_{2.5}$ of monthly afternoon times showed smaller increases right over the center of the fire area, and increased up to 40 μg m^{-3} during afternoon times on 31 October. At night, land breeze is enhanced by the decrease of land surface temperature due to the smoke radiative effect during daytime.

3. Over land, the smoke semi-direct effect is important in daytime as it increases stability and reduces the cloud cover, but has virtually zero effect at night. Over the Malaysian Peninsula, Sumatra Island and Borneo

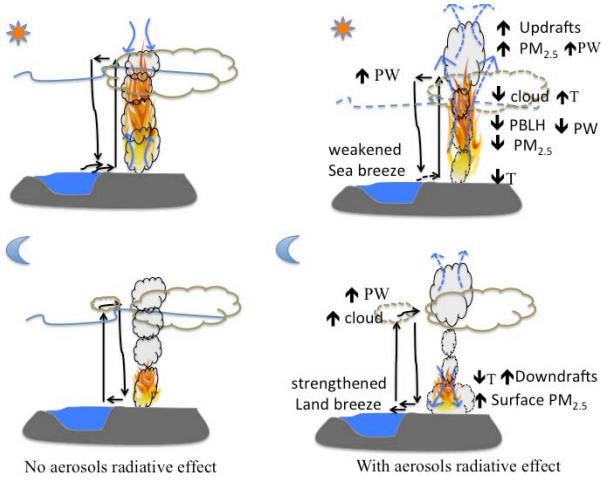

Fig. 11. A conceptual model that illustrates the radiative effect of smoke aerosols on the change of aerosol concentration, PBLH, wind, and cloud fraction over the Southeast Asian Maritime Continent. ↑ denotes increase, and ↓ denotes decrease. See the text in Sect. 5 for details.

Island, the monthly averaged low-level cloud fraction during daytime is decreased by more than 10 %, and a 40 % decrease can be found over Borneo during the afternoon of 31 October. Over the Karimata Strait, the change in the low-level wind pattern induced by the convergence caused an increase in cloud fraction in both daytime and nighttime. The decreased sea breeze during afternoon times can lead to a prominent increase of as much as 40 % in low-level clouds over coastal waters.

The conceptual model is presented in Fig. 11 to illustrate the radiative effect of smoke aerosols on above-discussed processes.During daytime (top row), the smoke-induced local convergences over the smoke source region, which transport more smoke particles above, renders a positive effect. During nighttime, however, this elevated smoke layer is decoupled from the boundary layer, and the local divergence enhances the downdraft and hence leads to the increase of smoke particles near the surface. The cloud change over continents mostly occur during the daytime over the fire area, where the low-level cloud fraction decreases due to the more stable PBL and the enhanced solar heating by smoke particles within and above clouds. However, during night (bottom row), the change of local wind (including sea breeze) induced by the radiative effect of smoke lead to a more convergence over the Karimata Strait and the south coastal area of Kalimantan during the nighttime; hence cloud fraction increases.

A multi-scale and multi-year analysis of modeling and field campaign data is needed to further evaluate the conceptual model proposed in this study. The unique topographical and geographical layout of the Southeast Asian Maritime Continent requires an integrated use of both the data and the modeling tools to resolve the processes at the local and regional scales toward a fuller understanding of smoke direct and indirect effects in that region. In addition, large interannual variations of fire activities were found over the southeastern Asia region, although high cloud cover in this region is persistent even in the dry season (Reid et al., 2012). Hence, we expect that the conceptual model in Fig. 11 can be generalized for other years in this region, although year-by-year variations of smoke can be more likely than those of clouds to lead to variations of the strength of each process in the conceptual model. Caution needs to be taken in applying this conceptual model to other tropical biomass burning regions such as the Amazon forest where significant change in cloud cover and resultant change in smoke radiative effects can be found between drier and wetter years (Yu et al., 2007).

Supplementary material related to this article is available online at http://www.atmos-chem-phys.net/14/159/2014/acp-14-159-2014-supplement.pdf.

Acknowledgements. This study is supported by the NASA Interdisciplinary Science Program managed by Hal. B. Maring. J. S. Reid's contribution was also partially supported by the NRL 6.1 base program. The authors gratefully acknowledge the Holland Computing Center of University of Nebraska – Lincoln and their staff, especially Adam Caprez, for their helpful efforts with modeling. Two anonymous reviewers are acknowledged for their careful reviews and constructive suggestions. The authors also express their gratitude to Eleanor Highwood for her editing and proofreading the manuscript.

Edited by: E. Highwood

References

Ackermann, I. J., Hass, H., Memmesheimer, M., Ebel, A., Binkowski, F. S., and Shankar, U.: Modal aerosol dynamics model for Europe: Development and first applications, Atmos. Environ., 32, 2981–2999, doi:10.1016/S1352-2310, 1998.

Akagi, S. K., Yokelson, R. J., Wiedinmyer, C., Alvarado, M. J., Reid, J. S., Karl, T., Crounse, J. D., and Wennberg, P. O.: Emission factors for open and domestic biomass burning for use in atmospheric models, Atmos. Chem. Phys., 11, 4039–4072, doi:10.5194/acp-11-4039-2011, 2011.

Andreae, M. O. and Merlet, P.: Emission of trace gases and aerosols from biomass burning, Global Biogeochem. Cy., 15, 955–966, doi:10.1029/2000GB001382, 2001.

Barnard, J. C., Fast, J. D., Paredes-Miranda, G., Arnott, W. P., and Laskin, A.: Technical Note: Evaluation of the WRF-Chem "Aerosol Chemical to Aerosol Optical Properties" Module using data from the MILAGRO campaign, Atmos. Chem. Phys., 10, 7325–7340, doi:10.5194/acp-10-7325-2010, 2010.

Bond, T. C. and Bergstrom, R. W.: Light absorption by carbonaceous particles: An investigative review, Aerosol Sci. Technol., 40, 27–67, 2006.

Campbell, J. R., Reid, J. S., Westphal, D. L., Zhang, J., Tackett, J. L., Chew, B. N., Welton, E. J., Shimizu, A., Sugimoto, N., and Aoki, K.: Characterizing the vertical profile of aerosol particle extinction and linear depolarization over Southeast Asia and the Maritime Continent: The 2007–2009 view from CALIOP, Atmos. Res., 122, 520–543, doi:10.1016/j.atmosres.2012.05.007, 2013.

Davison, P. S., Roberts, D. L., Arnold, R. T., Colvile, R. N.: Estimating the direct radiative forcing due to haze from the 1997 forest fires in Indonesia, J. Geophys. Res., 109, D10207, doi:10.1029/2003JD004264, 2004.

Duncan, B., Bey, I., Chin, M., Mickley, L., Fairlie, T., Martin, R., and Matsueda, H.: Indonesian wildfires of 1997: Impact on tropospheric chemistry, J. Geophys. Res., 108, 4458, doi:10.1029/2002JD003195, 2003.

Fast, J. D., Gustafson Jr., W. I., Easter, R. C., Zaveri, R. A., Barnard, J. C., Chapman, E. G., Grell, G. A., and Peckham, S. E.: Evolution of ozone, particulates, and aerosol direct radiative forcing in the vicinity of Houston using a fully coupled meteorology-chemistry-aerosol model. J. Geophys. Res., 111, D21305, doi:10.1029/2005JD006721, 2006.

Feng, N. and Christopher, S. A.: Satellite and Surface-based Remote Sensing of Southeast Asian Aerosols and their Radiative Effects, Atmos. Res., 122, 544–554, doi:10.1016/j.atmosres.2012.02.018, 2012.

Ghan, S. J., Laulainen, N. S., Easter, R. C., Wagener, R., Nemesure, S., Chapman, E. G., Zhang, Y., and Leung, L. R.: Evaluation of aerosol direct radiative forcing in MIRAGE, J. Geophys. Res., 106, 5295–5316, 2001.

Grell, G. A. and Dévényi, D.: A generalized approach to parameterizing convection combining ensemble and data assimilation techniques, Geophys. Res. Lett., 29, 1693, doi:10.1029/2002GL015311, 2002.

Grell, G. A., Peckham, S. E., Schmitz, R., McKeen, S. A., Frost, G., Skamarock, W. C., Eder, B.: Fully coupled 'online' chemistry in the WRF model, Atmos. Environ., 39, 6957–6975, 2005.

Hansen, J., Sato, M., Lacis, A., and Ruedy, R.: The missing climate forcing. Philos. T. Roy. Soc. London B, 352, 231–240, doi:10.1098/rstb.1997.0018, 1997.

Herner, J. D., Aw, J., Gao, O., Chang, D. P., and Kleeman, M. J.: Size and Composition Distribution of Airborne Particulate Matter in Northern California: I—Particulates Mass, Carbon, and Water-Soluble Ions, J. Air Waste Manag. Assoc., 55, 30–51, 2005.

Hong, S.-Y., Noh, Y., and Dudhia, J.: A new vertical diffusion package with an explicit treatment of entrainment processes, Mon. Weather Rev., 134, 2318–2341, doi:10.1175/MWR3199.1, 2006.

Hyer, E. J. and Chew, B. N.: Aerosol transport model evaluation of an extreme smoke episode in Southeast Asia, Atmos. Environ., 44, 1422–1427, 2010.

Hyer, E. J., Reid, J. S., Prins, e. M., Hoffman, J. P., Schmidt, C. C., Miettinen, J. I., and Giglio, L.: Patterns of fire activity over Indonesia and Malaysia from polar and geostationary satellite observations, Atmos. Res., 122, 504–519, doi:10.1016/j.atmosres.2012.06.011, 2012.

Jacobson, M. Z.: A physically-based treatment of elemental carbon optics: Implications for dlobal direct forcing of aerosols, Geophys. Res. Lett., 27, 217–220, 2000.

Kleeman, M. J., Schauer, J. J., and Cass, G. R.: Size and composition distribution of fine particulate matter emitted from motor vehicles, Environ. Sci. Technol., 34, 1132–1142, doi:10.1021/es981276y, 2000.

Koren, I., Kaufman, Y. J., Remer, L. A., Martins, J. V.: Measurement of the effect of Amazon smoke on inhibition of cloud formation, Science, 303, 1342–1345, 2004.

Koren, I., Martins, J. V., Remer, L. A., and Afargan, H.: Smoke invigoration versus inhibition of clouds over the Amazon, Science, 321, 946–949, 2008.

Levitus, S., Antonov, J. I., Boyer, T. P., Baranova, O. K., Garcia, H. E., Locarnini, R. A., Mishonov, A. V., Reagan, J. R., Seidov, D., Yarosh, E. S., and Zweng, M. M.: World ocean heat content and thermosteric sea level change (0–2000 m), 1955–2010, Geophys. Res. Lett., 39, L10603, doi:10.1029/2012GL051106, 2012.

Lim, H.-J. and Turpin, B. J.: Origins of Primary and Secondary Organic Aerosol in Atlanta: Results of Time-Resolved Measurements during the Atlanta Supersite Experiment, Environ. Sci. Technol., 36, 4489–4496, 2002.

Lin, Y.-L., Farley, R. D., and Orville, H. D.: Bulk parameterization of the snow field in a cloud model, J. Clim. Appl. Meteorol., 22, 1065–1092, doi:10.1175/1520-0450, 1983.

Liousse, C., Penner, J., Chuang, C., Walton, J., Eddleman, H., and Cachier, H.: A global three-dimensional model study of carbonaceous aerosols, J. Geophys. Res., 101, 19411–19419, doi:10.1029/95JD03426, 1996.

Mlawer, E. J., Taubman, S. J., Brown, P. D., Iacono, M. J., and Clough, S. A.: Radiative transfer for inhomogeneous atmospheres: RRTM, a validated correlated-k model for the longwave, J. Geophys. Res., 102, 16663–16682, doi:10.1029/97JD00237, 1997.

Ott, L., Duncan, B., Pawson, S., Colarco, P., Chin, M., Randles, C., Diehl, T., and Nielsen, E.: Influence of the 2006 Indonesian biomass burning aerosols on tropical dynamics studied with the GEOS-5 AGCM, J. Geophys. Res., 115, D14121, doi:10.1029/2009JD013181, 2010.

Podgorny, I., Li, F., and Ramanathan, V.: Large aerosol radiative forcing due to the 1997 Indonesian forest fire. Geophys. Res. Lett., 30, 1028, doi:10.1029/2002GL015979, 2003.

Ramanathan, V., Crutzen, P. J., Lelieveld, J., Mitra, A., Althausen, D., Anderson, J., Andreae, M., Cantrell, W., Cass, G., and Chung, C.: Indian Ocean Experiment: An integrated analysis of the climate forcing and effects of the great Indo-Asian haze, J. Geophys. Res., 106, 28371–28398, 2001.

Reid, J. S., Hobbs, P. V., Ferek, R. J., Blake, D. R., Martins, J. V., Dunlap, M. R., and Liousse, C.: Physical, chemical, and optical properties of regional hazes dominated by smoke in Brazil, J. Geophys. Res., 103, 32059–32080, doi:10.1029/98JD00458, 1998.

Reid, J. S., Koppmann, R., Eck, T. F., and Eleuterio, D. P.: A review of biomass burning emissions part II: intensive physical properties of biomass burning particles, Atmos. Chem. Phys., 5, 799–825, doi:10.5194/acp-5-799-2005, 2005a.

Reid, J. S., Eck, T. F., Christopher, S. A., Koppmann, R., Dubovik, O., Eleuterio, D. P., Holben, B. N., Reid, E. A., and Zhang, J.: A review of biomass burning emissions part III: intensive optical

properties of biomass burning particles, Atmos. Chem. Phys., 5, 827–849, doi:10.5194/acp-5-827-2005, 2005b.

Reid, J., Hyer, E., Prins, E., Westphal, D., Zhang, J., Wang, J., Christopher, S., Curtis, C., Schmidt, C., and Eleuterio, D.: Global monitoring and forecasting of biomass-burning smoke: Description of and lessons from the Fire Locating And Modeling of Burning Emissions (FLAMBE) program, Selected Topics in Applied Earth Observations and Remote Sensing, IEEE Journal, 2, 144–162, doi:10.1109/JSTARS.2009.2027443, 2009.

Reid, J. S., Xian, P., Hyer, E. J., Flatau, M. K., Ramirez, E. M., Turk, F. J., Sampson, C. R., Zhang, C., Fukada, E. M., and Maloney, E. D.: Multi-scale meteorological conceptual analysis of observed active fire hotspot activity and smoke optical depth in the Maritime Continent, Atmos. Chem. Phys., 12, 2117–2147, doi:10.5194/acp-12-2117-2012, 2012.

Reid, J. S., Hyer, E. J., Johnson, R., Holben, B. N., Yokelson, R. J., Zhang, J., Campbell, J. R., Christopher, S. A., Di Girolamo, L., Giglio, L., Holz, R. E., Kearney, C., Miettinen, J., Reid, E. A., Joseph Turk, F., Wang, J., Xian, P., Zhao, G., Balasubramanian, R., Chew, B. N., Janai, S., Lagrosas, N., Lestari, P., Lin, N.-H., Mahmud, M., Nguyen, X. A., Norris, B., Oahn, T. K., Oo, M., Salinas, S. V., Welton, E. J., and Liew, S. C.: Observing and understanding the Southeast Asian aerosol system by remote sensing: An initial review and analysis for the Seven Southeast Asian Studies (7SEAS) program., Atmos. Res., 122, 403–468, 2013.

Salinas, S. V., Chew, B. N., Miettinen, J., Campbell, J. R., Welton, E. J., Reid, J. S., Yu, L. E., and Liew, S. C.: Physical and optical characteristics of the October 2010 haze event over Singapore: A photometric and lidar analysis, Atmos. Res., 122, 555–570, 2013.

Schell, B., Ackermann, I. J., Hass, H., Binkowski, F. S., and Ebel, A.: Modeling the formation of secondary organic aerosol within a comprehensive air quality model system, J. Geophys. Res., 106, 28275–28293, doi:10.1029/2001JD000384, 2001.

Stockwell, W. R., Middleton, P., Chang, J. S., and Tang, X.: The second generation regional acid deposition model chemical mechanism for regional air quality modeling, J. Geophys. Res., 95, 16343–16316, doi:10.1029/JD095iD10p16343, 1990.

Stull, R.: Meteorology for scientists and engineers; second edition; Brooks/Cole, Pacific Grove, USA, 2000.

Tosca, M. G., Randerson, J. T., Zender, C. S., Nelson, D. L., Diner, D. J., and Logan, J. A.: Dynamics of fire plumes and smoke clouds associated with peat and deforestation fires in Indonesia, J. Geophys. Res., 116, D08207, doi:10.1029/2010JD015148, 2011.

van der Werf, G. R., Randerson, J. T., Giglio, L., Collatz, G. J., Kasibhatla, P. S., and Arellano Jr., A. F.: Interannual variability in global biomass burning emissions from 1997 to 2004, Atmos. Chem. Phys., 6, 3423–3441, doi:10.5194/acp-6-3423-2006, 2006.

Wang, J. and Christopher, S.: Mesoscale modeling of Central American smoke transport to the United States: 2. Smoke radiative impact on regional surface energy budget and boundary layer evolution, J. Geophys. Res., 111, 1–17, 2006.

Wang, J., Ge, C., Yang, Z., Hyer, E. J., Reid, J. S., Chew, B. N., and Mahmud, M.: Mesoscale modeling of smoke transport over the Southeast Asian Maritime Continent: interplay of sea breeze, trade wind, typhoon, and topography, Atmos. Res., 122, 486–503, 2013.

Wu, L., Su, H., and Jiang, J. H.: Regional simulations of deep convection and biomass burning over South America: 1. Model evaluations using multiple satellite data sets, J. Geophys. Res., 116, D17208, doi:10.1029/2011JD016105, 2011a.

Wu, L., Su, H., and Jiang, J. H.: Regional simulations of deep convection and biomass burning over South America: 2. Biomass burning aerosol effects on clouds and precipitation, J. Geophys. Res.-Atmos., 116, doi:10.1029/2011JD016106, 2011b.

Xian, P., Reid, J. S., Atwood, S. A., Johnson, R. S., Hyer, E. J., Westphal, D. L., and Sessions, W.: Smoke aerosol transport patterns over the Maritime Continent, Atmos. Res., 122, 469–485, 2013.

Yu, H., Fu, R., Dickinson, R. E., Zhang, Y., Chen, M., and Wang, H.: Interannual variability of smoke and warm cloud relationships in the Amazon as inferred from MODIS retrievals, Remote Sens. Environ., 111, 435–449, 2007.

Yu, H., Liu, S., and Dickinson, R.: Radiative effects of aerosols on the evolution of the atmospheric boundary layer, J. Geophys. Res., 107, 4142, doi:10.1029/2001JD000754, 2002.

Zhang, J. and Reid, J. S.: An analysis of clear sky and contextual biases using an operational over ocean MODIS aerosol product, Geophys. Res. Lett., 36, L15824, doi:10.1029/2009GL038723, 2009.

Zhang, Y.: Online-coupled meteorology and chemistry models: history, current status, and outlook, Atmos. Chem. Phys., 8, 2895–2932, doi:10.5194/acp-8-2895-2008, 2008.

Zhang, Y., Fu, R., Yu, H., Dickinson, R. E., Juarez, R. N., Chin, M., and Wang, H.: A regional climate model study of how biomass burning aerosol impacts land-atmosphere interactions over the amazon, J. Geophys. Res., 113, D14S15, doi:10.1029/2007JD009449, 2008.

Zhao, C., Liu, X., Leung, L. R., Johnson, B., McFarlane, S. A., Gustafson Jr., W. I., Fast, J. D., and Easter, R.: The spatial distribution of mineral dust and its shortwave radiative forcing over North Africa: modeling sensitivities to dust emissions and aerosol size treatments, Atmos. Chem. Phys., 10, 8821–8838, doi:10.5194/acp-10-8821-2010, 2010.